Elaboration and characterization of graphene-metal hybrid nanostructures
(NKFI K-119532, 2016.11.01 – 2021.10.31)
Principal Investigator: Dr. Zoltán Osváth, senior research fellow

The achievements of the project are summarized in the sections below:

1. Novel graphene/Sn hybrid nanostructures (*Carbon* 124, 611, 2017)

Graphene-covered Sn and SnO_x nanoparticles (NPs) were synthesized and characterized by atomic force microscopy (AFM), scanning tunneling microscopy (STM) and scanning tunneling spectroscopy (STS). We have shown that charge transfer occurs from Sn nanoparticles, inducing uniform doping of graphene (supported and suspended), which reduces significantly its environmental p-doping. Superconductivity induced to graphene by proximity effect from Sn nanoparticles has been observed at low temperatures of 0.5 K. We have shown that superconductivity is induced not only in supported graphene, but also in areas where graphene is suspended. The superconducting energy gap is enhanced in comparison to bulk tin due to the quantum size effect in Sn nanoparticles.

We have shown that the graphene overlayer protects Sn nanoparticles from oxidation. They melt during annealing at moderate temperatures and merge to form various larger nanostructures, including nanorods. Furthermore, we have shown that graphene facilitates the STM investigation of semiconducting SnO_x nanoparticles by fixing them to the HOPG substrate. We measured electronic band gaps of 2.7-3.2 eV for the SnO_x nanoparticles investigated by STS.

2. Interaction effects in a chaotic graphene quantum billiard (*Phys. Rev. B* 95, 075123, 2017)

Graphene quantum dots were synthesized by transferring graphene grown by chemical vapour deposition (CVD) onto highly oriented pyrolytic grafite (HOPG) and annealing the sample at 650 °C. At this temperature an important part of the graphene is removed by thermal oxidation, and small graphene quantum dots are produced on the substrate. We investigated such a graphene dot of 15 nm in diameter by STM and STS. We revealed by STM topographic superstructures corresponding to intervalley scattering, and to Umklapp processes. We pointed out that these results can be well understood by considering the electron-electron interaction in the quantum dot, accounting for both the measured density of state values by STS, and the observed topography patterns.

3. Anisotropic strain effects in small-twist-angle graphene on graphite (*Phys. Rev. B* 100, 125404, 2019)

We studied a small-twist-angle graphene on HOPG by STM/STS. We observed distorted moiré patterns with spatially dependent period. The nanoscale changes in the moiré period observed by STM reflected a locally strained graphene with anisotropic variation of the lattice parameter. We developed a combined graphical-numerical method in order to

evaluate the deformations that resulted in these distorted moiré patterns. As a result of our approach, the spatial dependence of the anisotropic deformations was revealed in unprecedented detail: not only the anisotropic moiré pattern could be reproduced, but also the local values of lattice parameters and misorientation angles could be accurately calculated. The sensitivity of the moiré pattern on the variation of graphene parameters was also demonstrated. Additionally, a local density of states (DOS) peak at the Dirac point was observed by room temperature STS measurements, localized at the protruding sites of the moiré pattern, which resulted in a significant increase of the apparent moiré corrugation. These findings were supported by classical molecular dynamics (CMD) simulations, which also revealed direction-dependent bond alternation patterns around the stackings, induced by shear strain. Density functional theory (DFT) calculations confirmed that the measured local DOS peak can be attributed to AAB-stacked trilayer regions in small-twist-angle graphene/HOPG systems. These findings may have implications in the nanoscale strain engineering of the atomic and electronic properties of graphene-based van der Waals heterostructures.

4. Large-wavelength second-order moiré pattern in graphene/Au(111)

Previously, we have revealed STM investigations of anomalously large moiré patterns forming in graphene/Au(111) heterostructures (Carbon 107 (2016) 792-799). While the introduction of significant strain (up to 3% expansion in graphene and up to 7% shrinkage in the gold topmost layer) can indeed induce theoretically large moiré wavelengths, in the context of the present work, we also established and examined a feasible explanation through second-order moiré patterns without the need of such external strain. The existence and the properties of higher-order patterns were shown in detail in [New J. Phys. 16 (2014) 083028] for optical moiré, however, no experimental or theoretical work was carried out to this date to elucidate the role of these patterns in real van der Waals heterostructures, especially in STM measurements.

Higher-order patterns realize when Fourier-overtones of lattice periodic quantities of the underlying lattices get close to each other in k-space. Due to the heavily decreasing Fourier-amplitude of the overtones, these higher-order patterns are very faint in the optical moiré. However, their effect in the case of atomic lattices through adhesion and electronic structure was not examined up until now. In this work, we studied these second-order moiré patterns in atomic lattices using theoretical calculations and atomistic simulations. It was already known that the wavelength of the first-order moiré pattern based on the fundamental harmonics has its minimum at 30°, which becomes such small that is comparable to the lattice constants. Therefore, it was usually expected for many van der Waals heterostructures that at rotation angle of 30° the corrugation is very low and no geometrical moiré pattern can be observed on STM images. In this work we showed that second-order patterns can change this picture remarkably for graphene/Au(111) systems, resulting in long wavelength moiré superlattices with significant corrugation at twist angles around 30°. A manuscript reporting these results is under preparation.

5. Adhesion model of graphene islands on metal substrates based on Moiré-patterns

Graphene grown on metal substrates often results rotational domains separated by grain boundaries. An interesting feature of this aspect is that several rotational angles are highly preferred by the graphene/metal system. We showed that this is related to the adhesion of the graphene to the metal substrate, which oscillates in the function of the rotational angle. We developed a continuum mathematical model that calculates the adhesion energy of a graphene island with a given size and orientation, only by knowing the underlying moiré-pattern that is formed between the atomic lattices. This approach agrees surprisingly well with DFT and CMD simulations.

6. Minigaps and pseudo-magnetic field in corrugated graphene

The moiré patterns formed on graphene/metal systems introduce slight periodic corrugation in graphene and thus periodic bond alternation. This Kekulé distorsion, the 2D analogue of Peierls distortion, breaks the chiral symmetry in graphene and leads to gap opening. We studied this effect in detail on graphene nanodomes by first principles DFT calculations. A considerable gap opening (up to 0.7 eV) has also been explored in the flat Kekulé distorted graphene. Comparing nanodomes with different height and width we find that gap opening is governed by the aspect ratio (height/width) leading to regimes with Dirac, semiconducting and flat band electronic structures.

7. Investigation of tip-selectively surface-modified gold nanorods (*J. Phys. Chem*. C 122, 1706-1710, 2018)

We investigated the patch formation of cysteamine (tip) and thiol-functionalized methoxy-polyethylene glycol (mPEG-SH) (side) coated gold nanorods at the ensemble and single particle levels. While cysteamine allows to optically monitor the ligand exchange process due to its significantly smaller size compared to cetyltrimethylammonium bromide (CTAB), the PEG grafted chemically to the rod surface provides the necessary stability of the particles during sample preparation and handling. The aim of the investigations was to shed light on the process of the cysteamine patch development at the gold nanorod tips, that is, on how localized patches developed when different amounts of cysteamine were used. We relied on optical spectroscopy, since the optical absorption or scattering spectrum of the nanorods depends heavily on the dielectric properties of the near-field region. Atomic force microscopy (AFM) allowed the direct visualization of the nanoparticles and to reconstruct their surface composition. Measurements performed on individual gold nanoparticles provided direct experimental evidence on the inhomogeneous ligand distribution of tip-selectively cysteamine-modified gold nanorods. At higher cysteamine concentration, a well-defined patch was formed at the tips of 115 × 55 nm gold nanorods. While at lower cysteamine concentration binding of the cysteamine still takes place at the rod tips, it only provides a partial coverage, allowing other thiol molecules to bind at the rod tip. The findings allow for a more rational design of functional patchiness at the nanoparticle level.

Finally, single particle spectroscopy and AFM was used to characterize the same gold nanorods with and without graphene coating, dispersed on glass substrates with metallic marks. The observed redshift of the optical spectra was unambiguously ascribed to the covering graphene layer.

8. Tuning the nanoscale rippling of graphene with PEGylated gold nanoparticles and ion irradiation (*Carbon Trends* 5, 100080, 2021)

Monolayers of Au nanoparticles with diameter of 18 nm, coated with mPEG-SH were prepared by interfacial assembly. High surface coverage of the NPs was obtained on Si(111) substrates by compressing the trapped monolayer in a Langmuir film balance. Graphene was transferred onto the nanoparticle monolayer. The resulting hybrid material was characterized by Raman spectroscopy, AFM, STM, and STS. We found that the Raman peaks of graphene were not enhanced on the surface-modified nanoparticle monolayer (absence of surface enhanced Raman scattering). This effect was attributed to the mPEG molecules, which increase the distance between graphene and the NPs.

AFM and STM measurements showed that the nanoparticle monolayer formed a quasi-continuous regular (hexagonal) pattern, with period of 20 nm, which is comparable to the periods observed in the moiré superstructures of small-twist-angle graphene bilayers. If such structural periodicity is induced in graphene, the local density of states can significantly change. The quasi-continuity of the nanoparticle monolayer means that there were voids in the layer, corresponding typically to 10 – 50 missing nanoparticles. There, suspended and curved graphene was observed, as it bridged the nanoparticle voids. The ratio between the depth and the diameter of these bowl-like graphene areas was between 5 and 10%. Previously, we used annealing at 400 °C to improve the adhesion of graphene to nanoparticles, and thus to increase its nanoscale rippling. In this case, however, annealing at this temperature induces the transformation of the NPs into larger ones, and thus the regular pattern of the as-prepared nanoparticle monolayer is lost. In order to tune the nanoscale rippling of graphene to match the periodicity of nanoparticles, we introduced point defects in the graphene structure by irradiation with 1 keV Ar^+ ions using a fluence of the order 10^{12} ions/cm^2. We took advantage of recent findings reported in the literature [e.g. Phys. Rev. B 89 (2014) 201406(R)], which showed that point defects not only modify the local density of states but also induce local deformations in the lattice near the defect. We presumed that sufficiently high density of point defects can tune the nanoscale corrugation of the whole graphene sheet. STM investigations of the graphene/m-PEG/Au NPs hybrid structure performed before and after irradiation revealed that indeed, the rippling of graphene was changed by irradiation and it approximated the periodicity of the underlying nanoparticle monolayer. Furthermore, we observed the signatures of individual point defects by atomic resolution STM, and showed by STS the modified local density of states near defect sites.

9. Gold nanorod plasmon resonance damping effects on a nanopatterned substrate (*J. Phys. Chem. C* 122, 24941–24948, 2018)

Plasmon-based devices and future optoelectronic integration require the attachment of metal nanocrystals onto various substrates, which generally breaks the symmetry of the dielectric environment surrounding the nanoparticles. Here, the understanding of surface damping and chemical interface damping processes as well as quality factor change for the supported nanoparticles becomes especially important. An approach to nanoscale manipulation is to break the lateral homogeneity of the substrate, for example, by its patterning with charged particle (ion or electron) beams.

In this work, silica nanosphere lithography combined with Xe+ ion irradiation was used to create high-contrast patterns on indium tin oxide (ITO). The structural, physical, and chemical properties of the substrate was modified on the nanoscale by ion bombardment performed through a nanomask of ordered colloidal silica nanospheres. The gold nanorods were distributed on the patterned ITO surface by spin-casting onto the substrates from a diluted solution, applying 1000 rpm for 30 s and dried under nitrogen flow. Two special cases were investigated in detail to account for the effect of local substrate inhomogeneity on the optical properties: when the particles connected two masked areas ("bridging") or when the particles were overlapping the boundary between the masked and irradiated areas ("overlapping"). Because of the high contrast of the surface modification method, the effect of local environment change in these special cases could be studied on a shorter length scale than the gold nanorod length. We showed that for gold nanorods the damping parameter is very sensitive to the nature of short-range local environment change, and the different behaviour for the symmetric "bridging" and the asymmetric "overlapping" cases was revealed.

In the asymmetric case, even if only one of the two tips was located on irradiated area (corresponding to approximately 1/3 of the total nanorod length) the damping was found to be the same as for a nanorod fully located on irradiated ITO. For the symmetric case, on the contrary, a more continuous increase of damping with the extent of inhomogeneity could be inferred. With the appearance of substrate inhomogeneity, the intensity variation followed the expected trend, but its change was not completely simultaneous with the change of damping. This behaviour is different than found for gold nanorods homogeneously surrounded by molecular coatings, where the intensity and line width change in a strongly coupled manner, as predicted by the classical damped harmonic oscillator model.

10. Dynamic strain in gold nanoparticle supported graphene induced by focused laser irradiation (*Nanoscale* 10, 13417-13425, 2018)

Thin gold films of 5 nm were deposited onto a SiO_2 (285 nm)/Si substrate by using an electron-beam evaporation system. Gold nanoparticles were formed on areas of 5 × 5 μm^2 by local laser heating of the gold layer using a confocal Raman microscope and a focused, 6 mW laser-power @ 633 nm. The laser beam was focused into a wavelength-wide spot and scanned over the selected 5 × 5 μm^2 regions with 20 × 20 points and a dwelling time of 3 seconds in each point. Graphene grown by chemical vapour deposition was transferred onto the substrate (gold layer and gold nanoparticles) using thermal release tape. For

comparison, we prepared a sample where graphene was transferred directly to a standard, SiO_2 (285 nm)/Si substrate. The samples were investigated by confocal Raman microscopy using excitation lasers of 488 and 633 nm. Low laser powers (0.6 mW) were used to characterize the same areas both before and after local heating. Raman maps were recorded in order to study the spatial distribution of spectral peaks. In this technique the excitation laser was scanned in a defined geometry and a complete Raman spectrum was recorded in every stepping point. We demonstrated that dynamic strain could be induced in the gold nanoparticle supported graphene by 6 mW laser irradiation, an effect which was completely reversible upon switching off the laser. We also showed that – while similar laser irradiation induced increased doping and damage in SiO_2/Si supported graphene – no change in doping or defect concentration was observed on Au NP-supported graphene, even after several irradiation cycles. Our findings can gain importance in local heat-assisted applications like plasmonic sensors, spasers, or photothermal therapy with nanoparticles or graphene/nanoparticle hybrids.

11. Preparation and characterization of graphene-silver nanoparticle hybrids on SiO_2 substrates

Thin (5 nm) silver layers were deposited on SiO_2 substrates. Silver nanoparticles were prepared by annealing the deposited thin film at 400 ^oC in argon atmosphere for 90 minutes. The annealing resulted in the formation of hemispherical nanoparticles with high surface coverage and diameters around 20 nm. Graphene grown on copper foil by chemical vapour deposition was transferred on the top of these NPs using thermal release tape and an aqueous solution of $CuCl_2$ (20%) and HCl (37%) to etch the copper. The resulting graphene-silver hybrid nanostructures were characterized by AFM and confocal Raman spectroscopy. It is known that a thin layer of Ag_2S forms on the surface of silver upon exposure to ambient conditions. We showed that the local heating induced by the laser beam of the Raman instrument decomposed this thin layer of Ag_2S, and this could be monitored *in-situ* on the measured Raman spectra. On graphene-covered NPs we observed more intense graphene Raman peaks (SERS effect), for example the intensity of graphene 2D peak was 8 times larger (after background removal) compared to the graphene 2D peak measured on SiO_2 substrate (Fig. 1a).

Raman measurements performed with higher laser intensity (6 mW) induced a dynamic hydrostatic strain (0.23% on average) in the graphene covering the silver NPs, which turned out to be completely reversible upon switching back to measurements using lower (1 mW) laser intensity (Fig. 1b). This effect is similar to what we observed and described earlier on graphene/gold nanoparticle hybrid structures [A. Pálinkás, et al., Nanoscale 10 (2018) 13417].

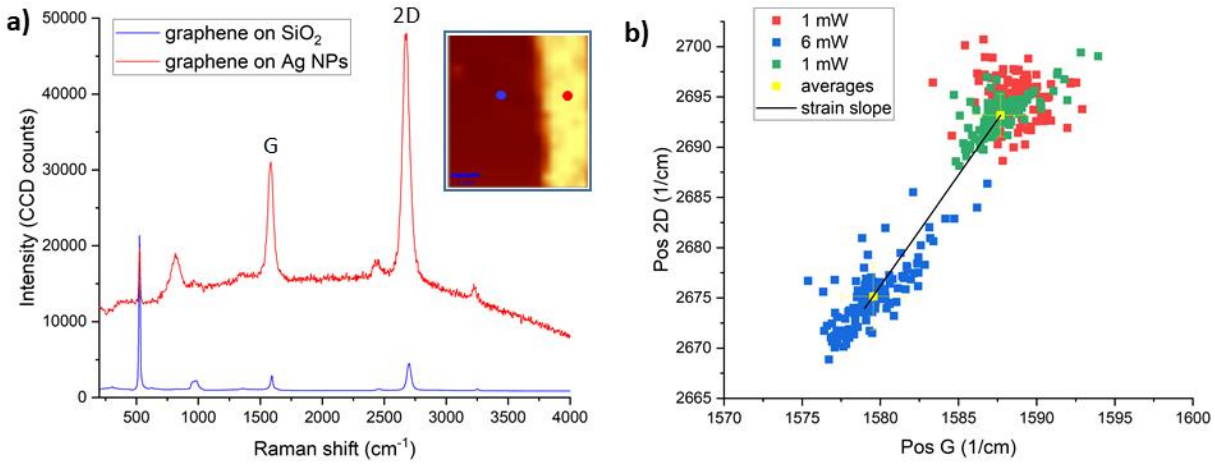

Figure 1. *(**a**) Comparison of graphene Raman spectra measured on SiO_2 substrate (blue line, blue symbol in the inset) and on Ag NPs (red line, red symbol in the inset). The inset shows the Raman map of graphene 2D peak measured on 4x4 μm^2 area. The area with darker contrast (lower peak intensity) corresponds to graphene on SiO_2 substrate, while the light contrasted area (higher peak intensity) corresponds to graphene on top of Ag NPs. (**b**) Correlation plot constructed from the position G and 2D peaks measured on graphene supported by Ag NPs. Red and green symbols demark low laser intensity (1 mW) measurements performed before (red) and after (green) higher laser intensity (6 mW) measurements marked by blue symbols. The shift of the average values is along the theoretical "strain" line (black).*

12. Synthesis and characterization of graphene-silver nanoparticle hybrids on HOPG substrates (*Materials* 13, 4660, 2020)

Thin silver films of 7 nm nominal thickness were evaporated onto HOPG substrates. Immediately after silver deposition and opening of the vacuum chamber, the thin silver films were covered with CVD graphene using transfer release tape. In order to drive the surface diffusion of deposited silver and to form Ag NPs, subsequent annealing of both bare and graphene-covered thin silver films was performed at 400 °C under inert gas (Ar) atmosphere for 90 minutes. We used these annealing parameters that worked earlier for the preparation of gold nanoparticles. The structure and physical properties of the prepared Ag NPs and graphene/Ag NP hybrids were investigated by tapping mode AFM, UV-Vis reflectance spectroscopy, scanning electron microscopy (SEM) and energy-dispersive X-ray spectroscopy (EDX). The graphene-silver nanohybrids were also characterized by STM and STS. We compared the differential current-voltage characteristics of HOPG-supported and silver-supported graphene, and we were able to reveal the local *n*-type electrostatic doping of graphene due to charge transfer from silver.

Annealing of the silver thin film resulted in the formation of silver nanoislands with heights around 20 nm and horizontal diameters of 100 nm. We showed that in the case of a graphene overlayer the Ag NPs tend to coalesce and to form larger nanoparticles. We demonstrated that a graphene overlayer preserves the local surface plasmon resonance (LSPR) of Ag NPs for at least three months, although the LSPR is gradually redshifted. This is three times longer than the LSPR of bare Ag NPs. We showed by SEM and EDX that graphene can protect Ag NPs from ambient sulphur for more than one year. Nevertheless, with the

applied transfer process, only 40 – 50% of Ag NPs were coated, and thus the observed loss of plasmonic properties is primarily attributed to the spontaneous sulfurization of non-covered nanoparticles. A way to improve the long-term stability of LSPR could be to increase significantly the total graphene coverage of Ag NPs.

13. Vapour sensing properties of graphene-covered metallic nanoparticles (*Nanoscale Advances* 1, 2408–2415, 2019)

Graphene-covered gold nanoparticles were produced, and their vapour sensing properties were investigated by measuring the LSPR shift of the gold NPs. We found that smaller, dome-like NPs were more sensitive to ethanol, isopropyl alcohol, and toluene vapours compared to slightly larger, flat NPs. The slope changes observed on the optical response curves of dome-like NPs could be well described by capillary condensation. The fast response and recovery of gold NPs were preserved on the graphene-covered samples as well. We demonstrated that the presence of a corrugated graphene overlayer increased the sensitivity to ethanol and isopropyl alcohol, while it decreased it towards toluene exposure (at concentrations ≥30%). Nevertheless, at low toluene concentrations (10%) where capillary condensation does not yet occur, the graphene covered NPs are more sensitive to toluene, compared to bare NPs. The detection mechanism based on refractive index change does not fully explain the induced LSPR shifts. The interactions between adsorbate, corrugated graphene, and the nanoparticles have to be considered.

Based on the above findings, similar research was performed with graphene-covered silver nanoparticles as well. Bare and graphene-covered Ag nanoparticles were prepared using the process described above in section 1. The optical reflectance properties of the samples were measured in the wavelength range of 200 to 1000 nm using an Avantes AvaSpec-HS1024 × 122TEC fibre optic spectrometer. We used a bifurcated probe for illumination and detection with 200 μm core diameters. The reflectance spectra of the samples were recorded by collecting the specular reflected light under normal incidence illumination with an Avantes AvaLight DH-S-BAL balanced UV-Vis light source. Well-defined local surface plasmon resonances are observed at 390 nm and 398 nm for bare and graphene-covered Ag nanoparticles, respectively. In addition, we prepared a graphene/Ag NPs sample which we treated in O_2 plasma for 5 s. The purpose of plasma treatment was to affect the sensing properties of graphene/Ag NPs by introducing large amounts of point defects into the structure of graphene. We examined the effect of plasma treatment by comparing the optical reflectance spectra measured before and after the treatment. Unexpectedly, the plasma treatment changed significantly the optical response of graphene-covered Ag NPs: its UV absorbance increased dramatically. The LSPR of the sample could be completely recovered by annealing at 400 °C under inert gas (Ar) atmosphere for 90 minutes. This healing effect is attributed to the decomposition of silver oxide, which probably had formed during the O_2 plasma treatment.

The graphene-covered Ag NPs were exposed to five different analytes independently: acetone, ethanol, 2-propanol (IPA), toluene, and water. The reflectance change of the samples occured in the LSPR region of the spectrum, between 350 and 450 nm which showed the vapour sensing capability of the graphene-covered Ag NPs. To investigate the sensitivity and chemical selectivity of the sample, ten different concentrations were applied during the vapour sensing measurement by diluting the saturated vapours of the five

analytes with artificial air. Note that the same vapour concentration of two different analytes caused different change in the optical response amplitude. This analyte-specific shift of the LSPR enables the use of these samples for chemically selective vapour sensors. The vapour sensing properties of plasma-treated (and then annealed) graphene/Ag NPs were very similar to the non-treated graphene/Ag NPs. This is tentatively attributed to the healing of graphene point defects through the applied annealing.

14. Density functional theory (DFT) calculations of metal-supported graphene with atomic defects

We have investigated the effect of the metal substrate on the electronic properties of graphene by using DFT calculations. In order to reveal the interactions between Au(111) and graphene, van der Waals density functional techniques were applied. First, we examined the interlayer distance between Au(111) and graphene and its effect on the electronic properties. For the relaxed interlayer distance, d=3.45 Ångström, the V-shape of graphene DOS is still present and only 150 meV *p*-doping occurs, in good agreement with our previous STS measurements. By decreasing the interlayer distance by 0.5 and 1 Ångström, stronger hybridization of the orbitals takes place, which leads to a metallic character of the graphene (see Fig. 2).

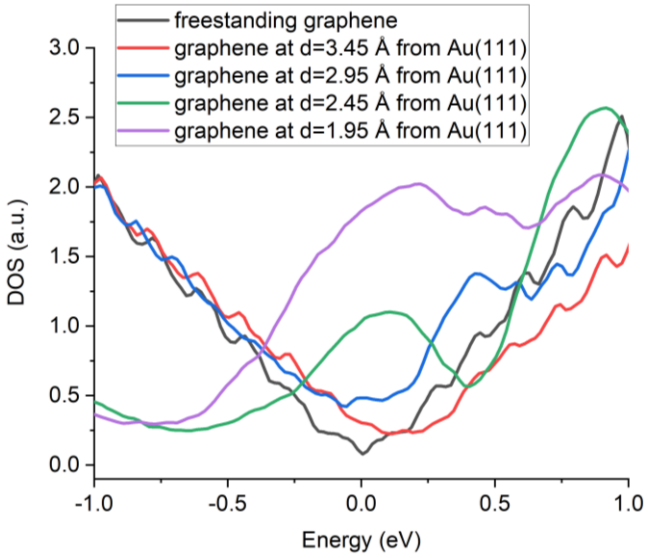

Figure 2. *Calculated DOS for freestanding graphene (black) and for gold-supported graphene at different graphene-Au(111) distances: 3.45 Å (red), 2.95 Å (blue), 2.45 Å (green), and 1.95 Å (magenta).*

The strongly modified DOS around the Fermi-level from these calculations resemble to the experiments of the annealed graphene/Au samples [A. Pálinkás, et al., Carbon 107 (2016) 792]. Therefore, we infer that thermal treatment can decrease the interlayer distance between Au and graphene, resulting modified electronic properties.

As a next step, we have considered an atomic defect, a single carbon atom vacancy in graphene (Fig. 3a). Previous DFT studies [PRL 107, 116803 (2011)] show vanishing magnetic moments of the vacancy due to the non-planar geometry of the relaxed graphene on Pt(111). In contrast, our calculations for Au(111) substrate show negligible out of plane

relaxation around the defect, preserving the 2D nature of graphene. In this case the magnetism is associated with the original σ- and π states of the C atoms surrounding the vacancy. The spin-polarized DOS of Au-supported graphene with vacancy is shown in Figure 3b. We observed 10% change of the magnetic moment of the vacancy in the presence of the Au(111) substrate compared to the graphene without substrate.

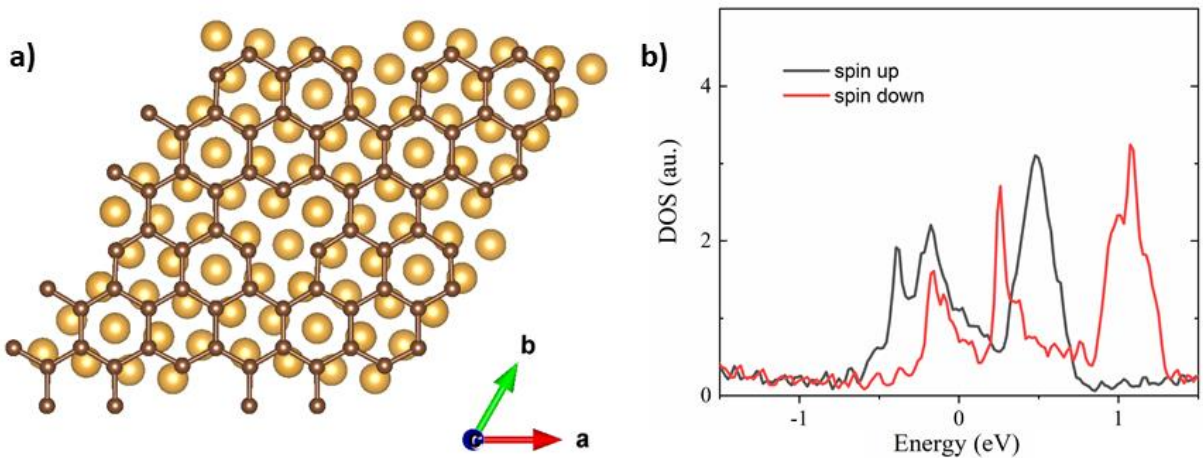

Figure 3. *(**a**) Model of graphene with single vacancy (3x3) on top of Au(111), used in the calculations. (**b**) Density of states for spin-up (black) and spin-down (red) states of the C atoms surrounding the vacancy.*

The slightly changed value of the momentum is originated from the Fermi-level shift caused by the Au(111) substrate [PRL 101, 026803 (2008)]. Similar small changes of the magnetic moment of graphene vacancy on Cu(111) has been reported previously [J. Appl. Phys. 113, 213709 (2013)], where the graphene geometry remained planar after the relaxation. The differences of the relaxation of graphene with vacancy on Pt, Au and Cu substrates could be explained by the different interlayer interactions. In the case of Au(111) and Cu(111) the binding energies are smaller compared to Pt(111), which can preserve the planar structure of graphene and the magnetic moment of the vacancy.

15. Higher-indexed Moiré patterns and surface states of $MoTe_2$/graphene heterostructure

In this study, graphene on n-type doped 6H-SiC(0001) was used as a substrate for the growth of $MoTe_2$ films. Following a vacuum graphitization process of 6H-SiC(0001) as detailed by Wang et al. [J. Phys.: Condens. Matter 25, 095002 (2013)], large-scale uniform double-layer graphene with the root mean square surface roughness of 0.1 - 0.2 nm was obtained. High crystalline quality of single-layer 2H-$MoTe_2$ films was formed on top of graphene by a multi-step molecular beam epitaxy (MBE) process as reported in a previous work [Appl. Surf. Sci. 523 (2020)]. After the 2H-$MoTe_2$ formation, sample was taken out of the MBE chamber and preserved in a clean dry box filled with nitrogen gas, then transferred to low-temperature STM working at 5 K.

Unusual higher-indexed Moiré patterns together with the periodicity of commensurate supercells were observed by STM in the $MoTe_2$/graphene heterostructure around 30° rotation angle (see Fig. 4). We found that these Moiré patterns depend delicately on the bias voltage of the STM. This was due to the high variability of the spatial distribution

of the charge density at different energies in the electronic surface states. This variability of the charge density is attributed to the competing contribution of Mo and Te orbitals during changing the energy (bias voltage), and also to the strong influence of the graphene substrate, as revealed by DFT calculations. The presence of the higher-indexed Moiré makes the apparent patterns unusually rich and complex, reflecting a highly crystalline $MoTe_2$/graphene heterostructure. The paper presenting this work was submitted and is currently under review at the journal *ACS Nano*.

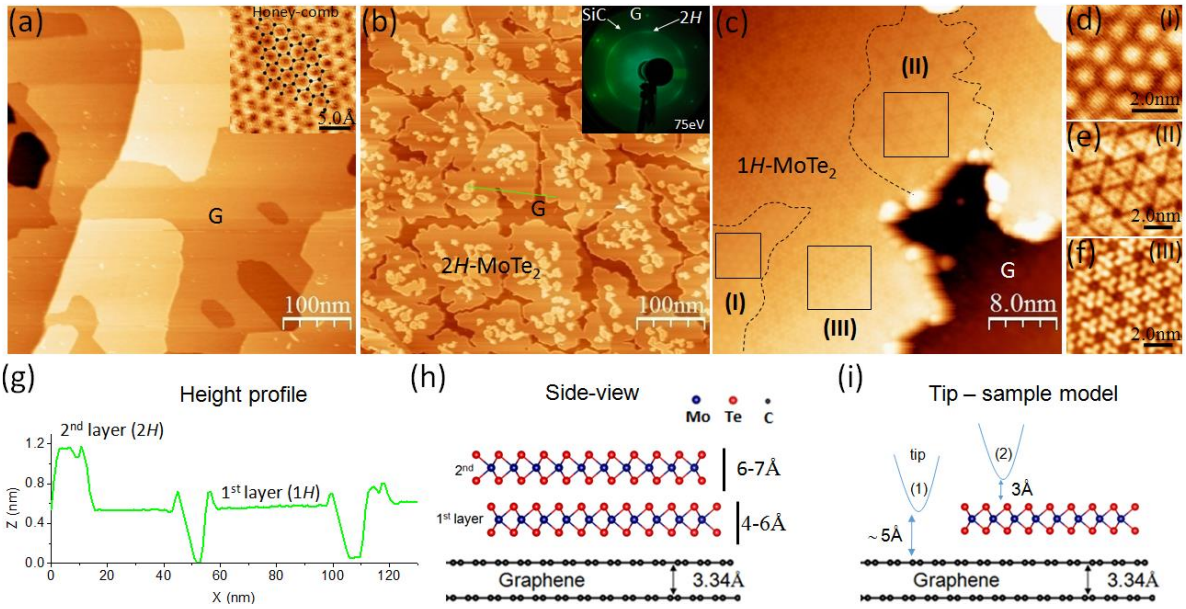

Figure 4. *STM images of (**a**) 500×500 nm² of bare graphene on terminated 6H-SiC(0001) substrate (V_{Sample} = +1 V, I_{Tunnel} = 800 pA) with an inset of the honey-comb structure, (**b**) after 2H-$MoTe_2$ formation taken on the same 500×500 nm² area (V_{Sample} = −0.6 V, I_{Tunnel} = 700 pA) with an inset of low-energy electron diffraction pattern and (**c**) 40×40 nm² of 1H-layer (V_{Sample} = +1 V, I_{Tunnel} = 5 pA), (**d**-**f**) Close-up observation of each Moiré pattern on local scan areas (I): $2\sqrt{3}R30°$, (II) $\sqrt{39}R33.1°$, and (III) $2\sqrt{7}R34.3°$ taken on the black squares of corresponding regions as marked on the STM image (c). (**g**) Height profile of 2H layer taken along the green line of pannel (b), (**h**) Schematic side view of 2H-$MoTe_2$ on graphene/6H-SiC(0001), and (**i**) Schematic view of the tip-sample geometry. "G" as marked on the STM images stands for graphene.*

PhD dissertations prepared during the project:

1. Pothorszky Szilárd: Régió-szelektíven felületmódosított arany nanorészecskék tervezett előállítása, vizsgálata és önszerveződése, BME VBK, Oláh György Doktori Iskola, PhD értekezés, 2017
2. Pálinkás András: Grafén-nanorészecske hibrid szerkezetek előállítása és vizsgálata pásztázószondás módszerekkel, BME TTK, Fizikai Tudományok Doktori Iskola, PhD értekezés, 2020
3. Szendrő Márton: Moiré-mintázatok modellezése kétdimenziós heteroszerkezetekben, ELTE TTK, Fizika Doktori Iskola, PhD értekezés, 2021 (to be defended soon)

BSc diploma work prepared during the project:

1. Kálvin György: Önrendeződő adszorbeátumok vizsgálata van der Waals-anyagok felületén, ELTE TTK, Fizika BSc szakdolgozat, 2021